MOLECULAR FORCES INVOLVED IN FORCE GENERATION DURING SKELETAL MUSCLE CONTRACTION

KENNETH P. MURPHY[1], YAN ZHAO[2] AND MASATAKA KAWAI[2],*

[1]Department of Biochemistry and [2]Department of Anatomy, The University of Iowa, College of Medicine, Iowa City, IA 52242, USA

Summary

Recent advances in protein chemistry and the kinetic analysis of tension transients in skeletal muscle fibres have enabled us to elucidate the molecular forces involved in force generation by cross-bridges. On the basis of the temperature effect, we conclude that the elementary step that generates force is an endothermic reaction (the enthalpy change $\Delta H°=124\,\mathrm{kJ\,mol^{-1}}$ at $15\,°C$), which accompanies a large entropy increase ($\Delta S°= 430\,\mathrm{J\,K^{-1}\,mol^{-1}}$) and a reduction in the heat capacity ($\Delta C_\mathrm{p}=-6.4\,\mathrm{kJ\,K^{-1}\,mol^{-1}}$). Thus, it can be concluded that the force-generating step is an entropy-driven reaction. The above results suggest that hydrophobic interactions are the primary cause of force generation, and that polar interactions (hydrogen bonding and charge interactions) are involved to a lesser degree. On the basis of the thermodynamic data, we estimate that during force generation approximately $50\,\mathrm{nm^2}$ of surface area is involved for hydrophobic interactions and another $30\,\mathrm{nm^2}$ for polar interactions. These data suggest that both the actomyosin interaction and the cleft closure of the myosin head are essential for force generation.

Key words: cross-bridge, temperature effects, enthalpy change, entropy change, hydrophobic interaction, polar interaction, accessible surface area, skeletal muscle.

Introduction

The elucidation of the mechanisms of force generation is an important milestone in understanding the molecular basis of muscle contraction. To identify intermediate states of hydrolysis and elementary reactions among various states, two methods have been employed: solution studies of extracted contractile proteins (Taylor, 1979; Eisenberg and Greene, 1980; Geeves *et al.* 1984) and studies of tension transients in muscle fibres (Pringle, 1967; Huxley and Simmons, 1971; Ford *et al.* 1977; Kawai and Brandt, 1980). These methods are complementary, and each method has strengths and weaknesses. While solution studies can give detailed information on various intermediate states of the cross-bridge cycle, the outcome of energy transduction (force) cannot be detected using this method. In muscle fibre studies, force can be measured but it is difficult to detect the elementary steps of contraction because multiple states are involved. Our method applies a high-resolution technique called 'sinusoidal analysis' to skinned muscle fibres (Pringle, 1967; Kawai and Brandt, 1980; Kawai and Halvorson, 1991) which takes advantage of both methods. The sinusoidal analysis method enables us to deduce details of the cross-bridge scheme and its rate and equilibrium constants (Kawai and Zhao, 1993; Zhao and Kawai, 1993, 1994). The use of skinned fibres enables us to apply chemical perturbations, so that hypotheses can be more rigorously tested than in intact preparations. By studying the temperature-dependence of the equilibrium constants, we obtain information on the molecular forces involved in the actin and myosin interaction which results in force generation.

In sinusoidal analysis, the length of single muscle fibres is perturbed with sine waves of varying frequencies and a low amplitude ($\pm1.6\,\mathrm{nm}$ per half-sarcomere). From the tension time course, the elastic modulus and viscous modulus of the fibres are obtained. The elastic modulus is the in-phase component of the tension change and the viscous modulus is the quadrature ($90°$ out of phase) component of the tension change, both with respect to the length change. Both quantities are standardized by using the length and the cross-sectional area of the fibres. The sinusoidal analysis method is in essence a mechanical equivalent of spectroscopy: when the viscous modulus is plotted against frequency (Fig. 1B), the modulus represents the amount of work absorbed by the preparation. We can characterize the property of a preparation by looking at a shift of the peak just as in spectroscopic analysis. What is interesting in muscle is that there is a frequency at which the viscous modulus becomes negative (see Fig. 1B); thereby, the

muscle generates work on the forcing apparatus. This quantity is called 'oscillatory work' (Pringle, 1967; Kawai and Brandt, 1980) and it includes information on the step that generates force (Kawai and Halvorson, 1991; Zhao and Kawai, 1994). Our focus in this paper is on how the characteristic frequency of oscillatory work changes with the phosphate concentration and temperature. In muscle fibres, inorganic phosphate (P_i) is known to perturb the force-generating step and its neighbouring reaction steps (Rüegg *et al.* 1971; Kawai and Halvorson, 1991; Fortune *et al.* 1991; Dantzig *et al.* 1992; Walker *et al.* 1992). From the temperature-dependence of the equilibrium constant, the entropy, enthalpy and heat capacity changes are obtained. These thermodynamic parameters can then be used to estimate the changes in hydrophobic and polar surface areas using empirically derived relationships (Murphy *et al.* 1992).

Materials and methods

Chemicals and solutions were prepared as reported in Zhao and Kawai (1994). The relaxing solution contained (in mmol l^{-1}): 6 EGTA, 2 MgATP, 5 free ATP, 8 potassium phosphate, 48 potassium propionate, 62 sodium propionate and 10 3-[N-Morpholino]propane-sulfonic acid (MOPS). The activating solutions used for the P_i study contained (in mmol l^{-1}): 6 CaEGTA, 5.3 MgATP, 4.7 free ATP, 15 creatine phosphate, 0–24 potassium phosphate ($K_{1.5}H_{1.5}PO_4$), 57–0 potassium propionate (compensated for the change in [potassium phosphate]), 25 sodium propionate, 10 MOPS and 160 units ml^{-1} of creatine kinase (CK). pCa ($=-\log[Ca^{2+}]$) of this solution was 4.82, pMg was 3.68 and [MgATP] was 5.0 mmol l^{-1}. The rigor solution contained (in mmol l^{-1}): 8 potassium phosphate, 76 sodium propionate, 103 potassium propionate and 10 MOPS. In all solutions used for experiments, ionic strength was adjusted to 200 mmol l^{-1} with sodium/potassium propionate and pH was adjusted to 7.00±0.01. The CK level was doubled for experiments at 25 °C and quadrupled for experiments at 30 °C. Chemically skinned psoas muscle fibres were prepared from rabbits as reported in Zhao and Kawai (1994). Preparations consisting of 2–3 fibres were isolated and used for experiments. The ends of the fibres were double-knotted, and each end was placed in a hook made of J-shaped tungsten wire with a gap of about 100 μm. One tungsten wire was connected to the length driver, and the other wire to the tension transducer assembly, as described in Zhao and Kawai (1994). The sarcomere length was adjusted to 2.5 μm. At the end of each experiment, rigor was induced from control activation, and the complex modulus of the rigor state was measured. A preliminary account of the present results was reported at a recent Biophysical Society Meeting (Zhao *et al.* 1996).

Results

Since sinusoidal analysis is a less commonly employed technique than time-course analysis to study cross-bridge
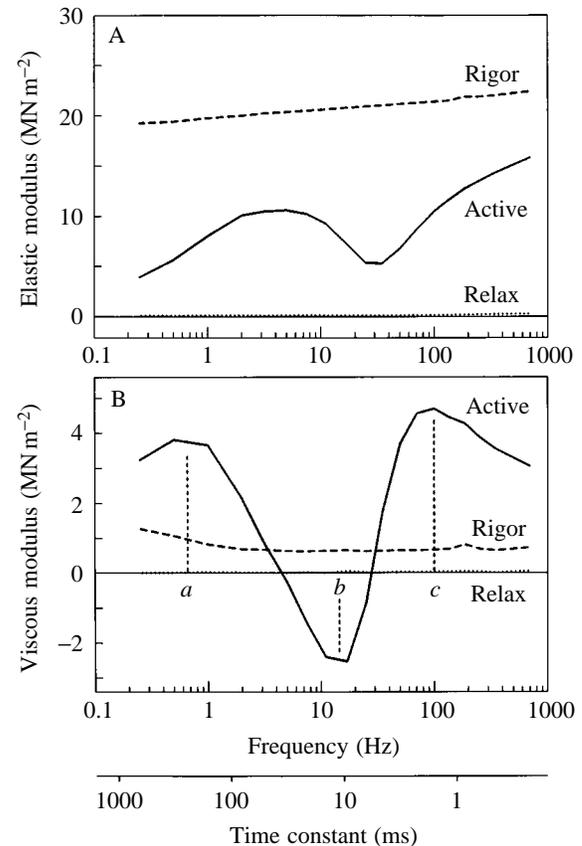

Fig. 1. The elastic modulus (A) and viscous modulus (B) plotted against frequency (in Hz) on a logarithmic scale. Also included below the abscissa in B is the corresponding time constant axis (in ms). Data were collected during relaxation (no Ca^{2+}), activation, and rigor (no ATP) as labelled. The measurements were carried out at 19 discrete frequencies (in Hz: 0.25, 0.5, 1, 2, 3.2, 5, 7.5, 11, 17, 25, 35, 50, 70, 100, 135, 187, 250, 350 and 700). The amplitude of length oscillation was ±1.6 nm per half-sarcomere. In B, *a*, *b* and *c* indicate the approximate locations of the characteristic frequencies associated with the viscous modulus of the activated preparation. Note that the viscous modulus is negative around the characteristic frequency *b*, where the muscle performs work on the length driver.

kinetics, an elaboration may be beneficial. The following experiments illustrate this analysis method. A preparation consisting of two fibres was initially relaxed in the relaxing solution. The preparation was then activated with the control activating solution that contained (in mmol l^{-1}): 6 CaEGTA, 5.8 MgATP, 1.36 ATP, 15 creatine phosphate, 8 potassium phosphate, 11 sodium propionate, 73 potassium propionate, 10 MOPS and 160 units ml^{-1} CK (pCa 4.66, pMg 3.30, pH 7.0). This was followed by two washes with the rigor solution. These experiments were carried out at 20 °C, 200 mmol l^{-1} ionic strength and with pH adjusted to 7.00. In each condition, sinusoidal analysis was carried out, and results are plotted in Fig. 1. Fig. 1A shows the elastic modulus and Fig. 1B shows the viscous modulus, both of which are plotted against frequency on a logarithmic scale. As seen in Fig. 1, the relaxed fibres do not have much
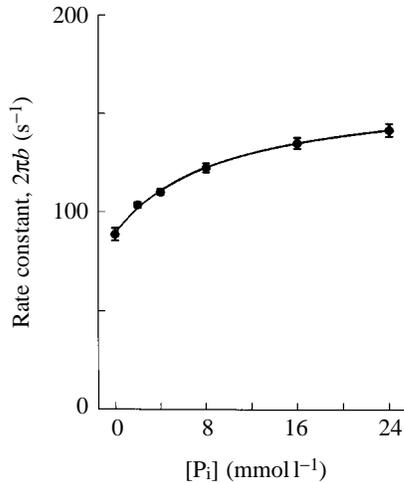
Fig. 2. The apparent rate constant $2\pi b$ is plotted against the phosphate (P_i) concentration. The experiment was carried out at 20 °C. The continuous line represents equation 1 with the best-fit parameters. The data are taken from Zhao and Kawai (1994).

elasticity or viscosity, indicating that cross-bridges are detached or weakly attached. The rigor fibres have a high elasticity and low viscosity, indicating that cross-bridges are strongly attached. In contrast, active fibres demonstrate complex spectra in both elastic and viscous moduli, indicating that cross-bridges are undergoing state changes. Under this condition, two positive peaks (at approximately 0.7 Hz and 100 Hz) and one negative peak (at approximately 14 Hz) are noticeable in the viscous modulus plot (Fig. 1B). These are labelled as the characteristic frequencies *a* (≈ 0.7 Hz), *b* (≈ 14 Hz) and *c* (≈ 100 Hz). When multiplied by 2π, they represent the apparent (=measured) rate constants. Their reciprocals are the time constants and are indicated below Fig. 1B. As seen in Fig. 1B, the three peaks are absent during relaxation or rigor, indicating that these peaks are characteristic of actively cycling cross-bridges.

Of the three frequencies, $2\pi b$ is the most interesting because work is produced at this frequency. By following the [P_i]-dependence of $2\pi b$, which increases and saturates as the P_i concentration is gradually raised from 0 to 24 mmol l^{-1} (Fig. 2), we are able to deduce the following cross-bridge scheme (Kawai and Halvorson, 1991; Zhao and Kawai, 1994):

$$\text{Step 4} \qquad\qquad \text{Step 5}$$

$$\text{AM.ADP.P}_i \underset{k_{-4}}{\overset{k_4}{\rightleftharpoons}} \text{AM*ADP.P}_i \underset{K_5}{\overset{\leftarrow}{\longrightarrow}} \text{AM*ADP} + \text{P}_i$$

where A is actin and M is myosin. K_5 is defined as the P_i association constant and k_4 and k_{-4} are rate constants. The analytical form of the apparent rate constant is (Kawai and Halvorson, 1991; Zhao and Kawai, 1993):

$$2\pi b = \sigma k_4 + \frac{K_5[\text{P}_i]}{1 + K_5[\text{P}_i]} k_{-4} . \qquad (1)$$

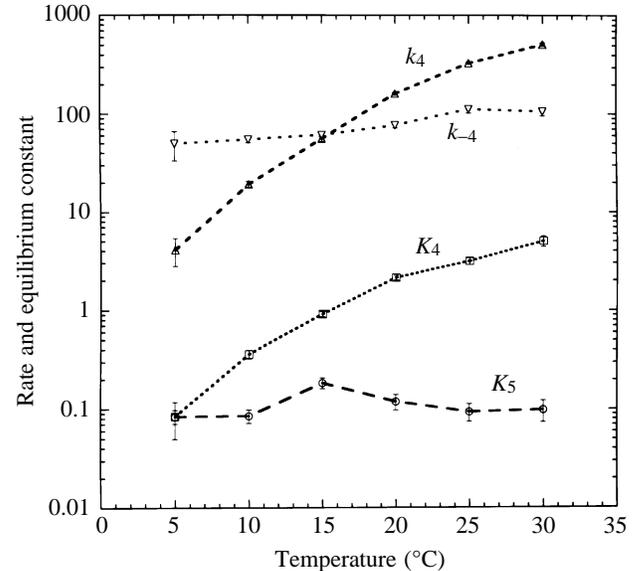The left-most state (AM.ADP.P$_i$) in the cross-bridge scheme is

Fig. 3. Temperature-dependence of the rate (k_4 and k_{-4}) and equilibrium (K_4 and K_5) constants. The units for k_4 and k_{-4} are s^{-1}, the units for K_5 are mmol l^{-1} and K_4 is unitless ($=k_4/k_{-4}$). Error bars indicate s.e.m. ($N=7$–8). The data points are connected by lines. Experiments were carried out on rabbit psoas fibres at 200 mmol l^{-1} ionic strength, pCa 4.82, 5 mmol l^{-1} MgATP, 15 mmol l^{-1} creatine phosphate, 160–640 units ml^{-1} creatine kinase and pH adjusted to 7.0. Data are reproduced from Zhao and Kawai (1994).

either a weakly attached or a detached state; the right-most state (AM*ADP) is strongly attached. There is now evidence that force generation occurs at step 4, which is an isomerization of the AM.ADP.P$_i$ state, and before P$_i$ is released. This conclusion is derived from the [P$_i$]-dependence of isometric tension in sinusoidal analysis (Kawai and Halvorson, 1991; Kawai and Zhao, 1993), pressure-release experiments (Fortune *et al.* 1991) and caged P$_i$ experiments (Dantzig *et al.* 1992; Walker *et al.* 1992) using rabbit psoas muscle fibres. The data in Fig. 2 are fitted to equation 1 to deduce the rate constants k_4 and k_{-4}, and the association constant K_5. The curved line in Fig. 2 was calculated using equation 1 with the best-fit parameters. σ in equation 1 is the factor which reflects that there is a rapid equilibrium to the left of the AM.ADP.P$_i$ state (Kawai and Halvorson, 1991; Zhao and Kawai, 1994). As seen in equation 1, σk_4 is the zero-intercept of Fig. 2, k_{-4} is the increment of $2\pi b$ from 0 to a large P$_i$ concentration and $1/K_5$ is the half-saturation point in Fig. 2.

To deduce thermodynamic parameters, we then studied the effect of temperature on k_4, k_{-4} and K_5. As shown in Fig. 3, k_4 is strikingly temperature-sensitive, whereas k_{-4} and K_5 are weakly temperature-sensitive. The equilibrium constant of the force generation step K_4 is equal to k_4/k_{-4} and is included in Fig. 3. As expected, K_4 increases significantly with temperature. From this observation, we conclude that the force-generating reaction is an endothermic reaction and absorbs heat. These results explain the large increase in isometric tension with temperature both during the steady state (Ford *et*
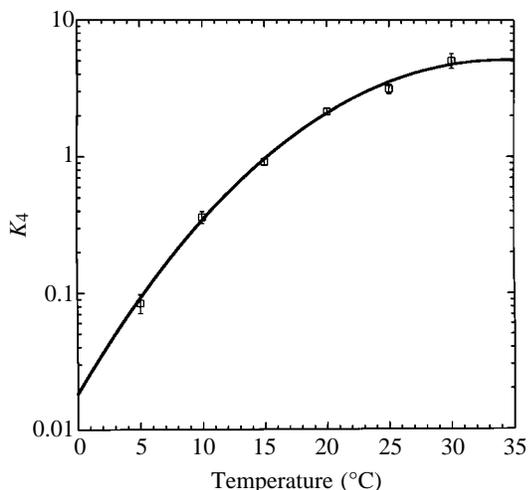
Fig. 4. The equilibrium constant K_4 and its fit to the modified van't Hoff equation (equation 2). The solid line is the best-fit of equation 2 to the data using the parameters listed in Table 1. The data were taken from Fig. 3.

al. 1977; Bressler, 1981; Ranatunga and Wylie, 1983; Zhao and Kawai, 1994) and after a sudden increase in temperature (Goldman *et al.* 1987; Bershitsky and Tsaturyan, 1989; Davis and Harrington, 1993). The data of Fig. 4 are fitted to the modified van't Hoff equation (see Appendix):

$$R\ln K_4 = -\Delta H^\circ_r/T + \Delta S^\circ_r + \Delta C_p[(T_r/T - 1) - \ln(T_r/T)], \quad (2)$$

where T is the absolute temperature, T_r is an arbitrary reference temperature (not a fitting parameter) and R is the gas constant. The derivation of equation 2 is found in the Appendix. $T_r=288$ K (15 °C) was chosen in this report, because it is close to the centre of the temperature range of our study. ΔH°_r and ΔS°_r are standard enthalpy and entropy changes at T_r, respectively. Equation 2 is the first-order expansion of the van't Hoff equation (equation A4, Appendix) at T_r, in which the temperature-sensitivity of ΔH° (equation A1) and ΔS° (equation A2) is considered. ΔC_p is the heat capacity change and represents the temperature coefficient of ΔH° (equation A3). In equation 2, ΔH°_r, ΔS°_r and ΔC_p are three unknown parameters to be determined experimentally.

The K_4 data from Fig. 3 are replotted on a magnified scale in Fig. 4. The number of total data points was 43. The data with all 43 points were fitted to equation 2 using a standard linear least-squares fitting program (note that equation 2 is linear with respect to three unknowns ΔH°_r, ΔS°_r and ΔC_p). The resulting best-fit curve is plotted in Fig. 4 and the best-fit values of ΔH°_r, ΔS°_r and ΔC_p along with their 95 % confidence ranges as determined from the fit are given in Table 1. For the calculation of 95 % confidence ranges, the facts that 43 data points were used and that there are three unknown parameters in equation 2 were considered. As seen in Fig. 4, the data fit equation 2 well and the three parameters can be determined accurately (Table 1). It should be noted here that ΔH°_r takes on a high positive value (124 kJ mol^{-1}), implying that the force-generating transition is an endothermic reaction. It is also

Table 1. *Thermodynamic parameters associated with the force-generation step (equilibrium constant K_4)*

Quantity	Best-fit value	95% confidence range	Units
ΔH°_r	124	±9	kJ mol^{-1}
ΔS°_r	430	±30	J K^{-1} mol^{-1}
ΔC_p	−6.4	±1.8	kJ K^{-1} mol^{-1}

ΔH°_r, standard enthalpy change at T_r, where T_r is an arbitrary reference temperature (15 °C); ΔS°_r, standard entropy change at T_r; ΔC_p, heat capacity change.

ΔH°_r and ΔS°_r are values at 15 °C.

ΔC_p is independent of temperature. The data in Fig. 4 were fitted to equation 2 using the standard linear least-squares method to find parameters ΔH°_r, ΔS°_r and ΔC_p.

95% confidence ranges of these parameters are also included.

evident that ΔS°_r has a high positive value (430 J K^{-1} mol^{-1}), implying that hydrophobic interactions are involved in force generation (Zhao and Kawai, 1994). Both ΔH°_r and ΔS°_r are larger than our previous estimates (103 kJ mol^{-1} and 357 J K^{-1} mol^{-1}, respectively; Zhao and Kawai, 1994), because the centre temperature of the previous estimate was about 18 °C (range 10–25 °C), which is higher than the current reference temperature (15 °C). If the current results are adjusted to 18 °C based on equations A1 and A2, then $\Delta H^\circ=105$ kJ mol^{-1} and $\Delta S^\circ=363$ J K^{-1} mol^{-1}. These values agree well with the previous estimate when the confidence ranges (±9 for ΔH°_r, ±30 for ΔS°_r; Table 1) of these values are taken into account.

When hydrophobic residues interact, the water molecules surrounding these residues lose structure, resulting in a large entropy increase (Frank and Evans, 1945; Sturtevant, 1977). Thus, high positive values of ΔH°_r and ΔS°_r imply that the force-generating transition is an entropy-driven, hydrophobic interaction. It should also be noted that ΔC_p has a high negative value (−6.4 kJ K^{-1} mol^{-1}) and is comparable to that observed for the folding of a 126-residue globular protein (Privalov and Gill, 1988). The negative value of ΔC_p is also indicative of hydrophobic interactions and implies that 'structured' water is removed (Frank and Evans, 1945).

It has been known for some time that the thermodynamics of the hydrophobic effect scale with the size of the hydrophobic molecule, in particular with the hydrophobic accessible surface area (Hermann, 1972; Gill and Wadsö, 1976; Chothia, 1976). More recently, it was learned that the energetics of hydrogen bonding in proteins can also be scaled with accessible surface area (Murphy and Freire, 1992; Spolar *et al.* 1992). These observations have led to empirical approaches to calculate the thermodynamics of protein unfolding transitions on the basis of changes in polar and apolar accessible surface areas (denoted ΔA_p and ΔA_{ap}, respectively). In this method, both ΔH° and ΔC_p are assumed to be linear combinations of contributions from ΔA_p and ΔA_{ap}. The linear coefficients are determined experimentally from model compounds and protein unfolding data. Using this

method, $\Delta H°$ and ΔC_p of protein unfolding can be accurately predicted from the protein structure (Murphy and Freire, 1992; Murphy, 1995).

This approach has recently been successfully applied to predicting the thermodynamics of protein–protein interactions including the binding of angiotensin II to a monoclonal antibody (Murphy *et al.* 1993), the dimerization of interleukin-8 (Burrows *et al.* 1994) and the binding of pepstatin to endothiapepsin (Gómez and Freire, 1995). The same method has also been used in a reverse sense to estimate ΔA_p and ΔA_{ap} from experimentally determined thermodynamic parameters (Murphy *et al.* 1995). In this case, the thermodynamics of binding of two different antibodies to cytochrome *c* was studied. It was shown that the estimated surface areas were in good agreement with estimates obtained from epitope mapping. In this report, we apply the same principle to estimate the structural changes associated with the force generation step (K_4). Because these interactions involve the same forces (hydrophobic and polar interactions) that are responsible for protein stability, this approach should provide reasonable estimates of accessible surface areas.

The change in heat capacity ($kJ\,K^{-1}\,mol^{-1}$) is related to changes in apolar (hydrophobic) and polar (electrostatic) accessible surface area (ASA, in nm^2) by equation 3 (Murphy and Freire, 1992):

$$\Delta C_P = (0.188\pm0.008)\Delta A_{ap} - (0.110\pm0.010)\Delta A_p, \quad (3)$$

where ΔA_{ap} is the change in apolar ASA, ΔA_p is the change in polar ASA and the coefficients are empirically determined from model compound dissolution studies (Murphy and Gill, 1991).

The change in enthalpy ΔH^* ($kJ\,mol^{-1}$), extrapolated to 100 °C, is proportional to ΔA_p (in nm^2) (Murphy and Freire, 1992):

$$\Delta H^* = (14.6\pm1.2)\Delta A_p. \quad (4)$$

Knowing the value of $\Delta H°$ and the value of ΔC_p (Table 1), we can then apply equations 3 and 4 to estimate values for ΔA_p and ΔA_{ap} (Murphy *et al.* 1995) (Table 2). The value of $\Delta H°$ extrapolated to 100 °C is $-420\pm160\,kJ\,mol^{-1}$ [from equation A1, $\Delta H^*=\Delta H°_r+\Delta C_p(100-15)$]. From equation 4, it follows that $\Delta A_p=-29\pm11\,nm^2$. Substituting this value into equation 3 and solving for ΔA_{ap} yields $-51\pm12\,nm^2$ of apolar surface area buried, consistent with a large hydrophobic contribution. The

Table 2. *Changes in accessible surface area predicted from the thermodynamics associated with the equilibrium constant (K_4) of force-generating step 4*

Quantity	Value	Units
ΔA_{ap}, change in apolar ASA	-51 ± 12	nm^2
ΔA_p, change in polar ASA	-29 ± 11	nm^2
ΔA_{tot}, change in the total ASA	-80 ± 16	nm^2

Values are best fit $\pm$ 95 % confidence ranges.
ASA, accessible surface area.

estimated total surface area change is $-80\pm16\,nm^2$. In this analysis, we have transformed two thermodynamic parameters ($\Delta H°$ and ΔC_p) into two parameters associated with structure (ΔA_{ap} and ΔA_p). We have similarly propagated the uncertainties associated with these parameters (Bevington and Robinson, 1992).

Discussion

The estimated changes in surface area provide insight into the structural effects that accompany force generation. The crystallographic structure of actin (Kabsch *et al.* 1990) indicates that globular actin is approximately disk-shaped with a diameter of 5.5 nm and a thickness of 3.5 nm, giving rise to a total surface area of approximately $110\,nm^2$. Thus, our calculated change in total ASA ($80\,nm^2$) is large when compared with the total actin surface area, although only approximately $40\,nm^2$ (=80/2) is applicable to actin, because two surfaces are involved in a macromolecular interaction. Evidently, a significant portion of this ASA must be located in the interface between the actin and myosin molecules. A recent computer-aided analysis (Rayment *et al.* 1993*a*) revealed that at least five hydrophobic amino acid residues on actin (Ala144, Ile341, Ile345, Leu349, Phe352) and at least eight hydrophobic amino acid residues on myosin (Pro529, Met530, Ile535, Met541, Phe542, Pro543, Tyr626, Gln647) are involved in the stereospecific and hydrophobic interaction when actin and myosin are brought into close proximity so that their contours fit to the three-dimensional reconstruction of the cryo-electron microscope images of F-actin decorated with subfragment-1 (Milligan *et al.* 1990). However, the combined ASA of these residues is approximately $16\,nm^2$, only 31 % of the ΔA_{ap} estimated here from the thermodynamic analysis. This would suggest either the presence of additional amino acid residues interacting in the actomyosin interface or the presence of a conformational change within the myosin head and/or in the actin molecule. Since 37 % of the actin surface area could not be used for the interaction with myosin, an additional conformational change within the myosin head and/or actin seems likely.

One possibility is a closure of the myosin 'cleft' upon force generation. This cleft exists between the upper 50 kDa domain and the lower 50 kDa domain in the heavy chain of the myosin head (Rayment *et al.* 1993*b*), and it must be closed for actin and myosin to interact (Rayment *et al.* 1993*a*). The closure of this cleft is believed to swing the C-terminal α-helical region of the myosin head, thus propelling the thick filament to cause force generation and filament sliding (Fisher *et al.* 1995). Our results are consistent with the hypothesis that cleft closure takes place simultaneously with force generation. It is not difficult to imagine that stereospecific interaction between amino acid residues would take place when the upper 50 kDa domain and the lower 50 kDa domain interact through cleft closure. These interactions would account for the large ASA indicated by the thermodynamic data.

In conclusion, our analysis indicates that force is generated simultaneously with the burial of a considerable surface area

of actin and myosin, especially of the hydrophobic surface, implying that hydrophobic interactions are the primary cause of force generation. Our analysis also indicates that the surface area associated with polar amino acid residues is involved to a lesser extent. Our analysis further implies that the actomyosin interface is not adequate to account for our data and an additional conformational change, such as the cleft closure of the myosin head, must accompany force generation. Although our analysis provides only an approximate sketch of the structural changes involved in force generation, it should be useful in further modelling of the molecular events that occur during actomyosin interaction and in elucidating the mechanism of force generation by cross-bridges.

Appendix

ΔH° and ΔS° are weakly temperature-dependent, and they can be expanded around a reference temperature T_r:

$$\Delta H^\circ = \Delta H^\circ_r + \Delta C_p(T - T_r), \tag{A1}$$

$$\Delta S^\circ = \Delta S^\circ_r + \Delta C_p(\ln T - \ln T_r), \tag{A2}$$

where

$$\Delta C_p = \left(\frac{\partial \Delta H^\circ}{\partial T}\right)_p = \left(\frac{\partial \Delta S^\circ}{\partial \ln T}\right)_p \tag{A3}$$

is the heat capacity change under the constant pressure (p). T_r is any reference temperature, and it can be arbitrarily selected. The standard van't Hoff equation is:

$$R\ln K = -\Delta H^\circ/T + \Delta S^\circ. \tag{A4}$$

By substituting ΔH° and ΔS° with equations A1 and A2, we obtain:

$$R\ln K = -\Delta H^\circ_r/T + \Delta S^\circ_r + \Delta C_p[(T_r/T - 1) - \ln(T_r/T)]. \tag{A5}$$

This is the modified van't Hoff equation (equation 2).

References

Bershitsky, S. Y. and Tsaturyan, A. K. (1989). Tension responses to joule temperature jump in skinned rabbit muscle fibres. *J. Physiol., Lond.* **447**, 425–448.

Bevington, P. R. and Robinson, D. K. (1992). *Data Reduction and Error Analysis for the Physical Sciences*. New York: McGraw-Hill.

Bressler, B. H. (1981). Isometric contractile properties and instantaneous stiffness of amphibian skeletal muscle in the temperature range from 0 to 20 °C. *Can. J. Physiol. Pharmac.* **59**, 548–554.

Burrows, S. D., Doyle, M. L., Murphy, K. P., Franklin, S. G., White, J. R., Brooks, I., McNulty, D. E., Scott, M. O., Knutson, J. R., Porter, D., Young, P. R. and Hensley, P. (1994). Interleukin-8 is a monomer at physiological concentrations: implications for its biological activity. *Biochemistry* **33**, 12741–12745.

Chothia, C. (1976). The nature of the accessible and buried surfaces in proteins. *J. molec. Biol.* **105**, 1–14.

Dantzig, J., Goldman, Y., Millar, N. C., Lacktis, J. and Homsher, E. (1992). Reversal of the cross-bridge force-generation transition by the photogeneration of phosphate in rabbit psoas muscle fibres. *J. Physiol., Lond.* **451**, 247–278.

Davis, J. S. and Harrington, W. (1993). A single order–disorder transition generates tension during the Huxley–Simmons phase 2 in muscle. *Biophys. J.* **65**, 1886–1898.

Eisenberg, E. and Greene, L. E. (1980). The relation of muscle biochemistry to muscle physiology. *Ann. Rev. Physiol.* **42**, 293–309.

Fisher, A. J., Smith, C. A., Thoden, J., Smith, R., Sutoh, K., Holden, H. M. and Rayment, I. (1995). Structural studies of myosin–nucleotide complexes: a revised model for the molecular basis of muscle contraction. *Biophys. J.* **68**, 19s–28s.

Ford, L. E., Huxley, A. F. and Simmons, R. M. (1977). Tension responses to sudden length change in stimulated frog muscle fibres near slack length. *J. Physiol., Lond.* **269**, 441–515.

Fortune, N. S., Geeves, M. A. and Ranatunga, K. W. (1991). Tension response to rapid pressure release in glycerinated rabbit muscle fibers. *Proc. natn. Acad. Sci. U.S.A.* **88**, 7323–7327.

Frank, H. S. and Evans, M. W. (1945). Free volume and entropy in condensed systems. III. Entropy on binary liquid mixtures; partial molal entropy in dilute solutions; structure and thermodynamics in aqueous electrolytes. *J. chem. Phys.* **13**, 507–532.

Geeves, M. A., Goody, R. S. and Gutfreund, H. (1984). Kinetics of acto-S1 interaction as a guide to a model for the cross-bridge cycle. *J. Muscle Res. Cell Motil.* **5**, 351–361.

Gill, S. J. and Wadsö, I. (1976). An equation of state describing hydrophobic interactions. *Proc. natn. Acad. Sci. U.S.A.* **73**, 2955–2958.

Goldman, Y. E., McCray, J. A. and Ranatunga, K. W. (1987). Transient tension changes initiated by laser temperature jumps in rabbit psoas muscle fibres. *J. Physiol., Lond.* **392**, 71–95.

Gómez, J. and Freire, E. (1995). Thermodynamic mapping of the inhibitor site of the aspartic protease endothiapepsin. *J. molec. Biol.* **252**, 337–350.

Hermann, R. B. (1972). Theory of hydrophobic bonding. II. The correlation of hydrocarbon solubility in water with solvent cavity surface area. *J. phys. Chem.* **76**, 2754–2759.

Huxley, A. F. and Simmons, R. M. (1971). Proposed mechanism of force generation in striated muscle. *Nature* **233**, 533–538.

Kabsch, W., Mannherz, H. G., Suck, D., Pai, E. F. and Holmes, K. C. (1990). Atomic structure of the actin:DNase I complex. *Nature* **347**, 37–44.

Kawai, M. and Brandt, P. W. (1980). Sinusoidal analysis: a high resolution method for correlating biochemical reactions with physiological processes in activated skeletal muscles of rabbit, frog and crayfish. *J. Muscle Res. Cell Motil.* **1**, 279–303.

Kawai, M. and Halvorson, H. R. (1991). Two step mechanism of phosphate release and the mechanism of force generation in chemically skinned fibers of rabbit psoas muscle. *Biophys. J.* **59**, 329–342.

Kawai, M. and Zhao, Y. (1993). Cross-bridge scheme and force per cross-bridge state in skinned rabbit psoas muscle fibers. *Biophys. J.* **65**, 638–651.

Milligan, R. A., Whittaker, M. and Safer, D. (1990). Molecular

structure of F-actin and location of surface binding sites. *Nature* **348**, 217–221.

MURPHY, K. P. (1995). Noncovalent forces important to the conformational stability of protein structures. In *Protein Stability and Folding* (ed. B. A. Shirley), pp. 1–34. Totowa, NJ: Humana Press.

MURPHY, K. P., BHAKUNI, V., XIE, D. AND FREIRE, E. (1992). The molecular basis of co-operativity in protein folding. III. Identification of cooperative folding units and folding intermediates. *J. molec. Biol.* **227**, 293–306.

MURPHY, K. P. AND FREIRE, E. (1992). Thermodynamics of structural stability and cooperative folding behavior in proteins. *Adv. Protein Chem.* **43**, 313–361.

MURPHY, K. P., FREIRE, E. AND PATERSON, Y. (1995). Configurational effects in antibody–antigen interactions studied by microcalorimetry. *Proteins* **21**, 83–90.

MURPHY, K. P. AND GILL, S. J. (1991). Solid model compounds and the thermodynamics of protein unfolding. *J. molec. Biol.* **222**, 699–709.

MURPHY, K. P., XIE, D., GARCIA, K. C., AMZEL, L. M. AND FREIRE, E. (1993). Structural energetics of peptide recognition: angiotensin II/antibody binding. *Proteins* **15**, 113–120.

PRINGLE, J. W. S. (1967). The contractile mechanism of insect fibrillar muscle. *Prog. Biophys. molec. Biol.* **17**, 1–60.

PRIVALOV, P. L. AND GILL, S. J. (1988). Stability of protein structure and hydrophobic interaction. *Adv. Protein Chem.* **39**, 191–234.

RANATUNGA, K. W. AND WYLIE, S. R. (1983). Temperature-dependent transitions in isometric contractions of rat muscle. *J. Physiol., Lond.* **339**, 87–95.

RAYMENT, I., HOLDEN, H. M., WHITTAKER, M., YOHN, C. B., LORENZ, M., HOLMES, K. C. AND MILLIGAN, R. A. (1993*a*). Structure of the actin–myosin complex and its implications for muscle contraction. *Science* **261**, 58–65.

RAYMENT, I., RYPNIEWSKI, W. R., SCHMIDT-BÄSE, K., SMITH, R., TOMCHICK, D. R., BENNING, M. M., WINKELMANN, D. A., WESENBERG, G. AND HOLDEN, H. M. (1993*b*). Three-dimensional structure of myosin subfragment-1: A molecular motor. *Science* **261**, 50–57.

RÜEGG, J. C., SCHADLER, M., STEIGER, G. J. AND MILLER, G. (1971). Effects of inorganic phosphate on the contractile mechanism. *Pflügers Arch.* **325**, 359–364.

SPOLAR, R. S., LIVINGSTONE, J. R. AND RECORD, M. T., JR (1992). Use of liquid hydrocarbon and amide transfer data to estimate contributions to thermodynamic functions of protein folding from the removal of nonpolar and polar surface from water. *Biochemistry* **31**, 3947–3955.

STURTEVANT, J. M. (1977). Heat capacity and entropy changes in processes involving proteins. *Proc. natn. Acad. Sci. U.S.A.* **74**, 2236–2240.

TAYLOR, E. W. (1979). Mechanisms of actomyosin ATPase and the problem of muscle contraction. *Crit. Rev. Biochem.* **6**, 103–164.

WALKER, J. W., LU, Z. AND MOSS, R. L. (1992). Effects of Ca^{2+} on the kinetics of phosphate release in skeletal muscle. *J. biol. Chem.* **267**, 2459–2466.

ZHAO, Y. AND KAWAI, M. (1993). The effect of lattice spacing change on cross-bridge kinetics in chemically skinned rabbit psoas muscle fibers. II. Elementary steps affected by the spacing change. *Biophys. J.* **64**, 197–210.

ZHAO, Y. AND KAWAI, M. (1994). Kinetic and thermodynamic studies of the cross-bridge cycle in rabbit psoas muscle fibers. *Biophys. J.* **67**, 1655–1668.

ZHAO, Y., MURPHY, K. P. AND KAWAI, M. (1996). Molecular forces involved in force generation during muscle contraction. *Biophys. J.* **70**, A126 (Abstr.).